J. Biochem. 2012;151(4):447–455 doi:10.1093/jb/mvs024

JB THE JOURNAL OF BIOCHEMISTRY

Human hematopoietic prostaglandin D synthase inhibitor complex structures

Received September 25, 2011; accepted December 27, 2011; published online March 13, 2012

Yuji Kado[1], Kosuke Aritake[2], Nobuko Uodome[2], Yousuke Okano[1], Nobuo Okazaki[1], Hiroyoshi Matsumura[1], Yoshihiro Urade[2] and Tsuyoshi Inoue[1,*]

[1]Department of Applied Chemistry, Graduate School of Engineering, Osaka University, 2-1 Yamada-Oka, Suita, Osaka 565-0871, Japan; and [2]Department of Molecular Behavioral Biology, Osaka Bioscience Institute, Suita, Osaka, 565-0874, Japan

*Tsuyoshi Inoue, Department of Applied Chemistry, Graduate School of Engineering, Osaka University, 2-1 Yamada-Oka, Suita, Osaka 565-0871, Japan. Tel: +81-6-6879-7408, Fax: +81-6-6879-7409, email: inouet@chem.eng.osaka-u.ac.jp

Protein Data Bank accession numbers
The atomic coordinates and structure factors of the complex with Cibacrone Blue and the complex with APAS have been deposited with the RCSB Protein Data Bank as 3VI7 and 3VI5, respectively.

In mast and Th2 cells, hematopoietic prostaglandin (PG) D synthase (H-PGDS) catalyses the isomerization of PGH_2 in the presence of glutathione (GSH) to produce the allergic and inflammatory mediator PGD_2. We determined the X-ray structures of human H-PGDS inhibitor complexes with 1-amino-4-{4-[4-chloro-6-(2-sulpho-phenylamino)-[1,3,5]triazin-2-ylmethyl]-3-sulpho-phenylamino}-9,10-dioxo-9,10-dihydro-anthracene-2-sulphonic acid (Cibacron Blue) and 1-amino-4-(4-aminosulphonyl) phenyl-anthraquinone-2-sulphonic acid (APAS) at 2.0 Å resolution. When complexed with H-PGDS, Cibacron Blue had an IC_{50} value of 40 nM and APAS 2.1 μM. The Cibacron Blue molecule was stabilized by four hydrogen bonds and π–π stacking between the anthraquinone ring and Trp104, the ceiling of the active site H-PGDS pocket. Among the four hydrogen bonds, the Cibacron Blue terminal sulphonic group directly interacted with conserved residues Lys112 and Lys198, which recognize the PGH_2 substrate α-chain. In contrast, the APAS anthraquinone ring was inverted to interact with Trp104, while its benzenesulphonic group penetrated the GSH-bound region at the bottom of the active site. Due to the lack of extended aromatic rings, APAS could not directly hydrogen bond with the two conserved lysine residues, thus decreasing the total number of hydrogen bond from four to one. These factors may contribute to the 50-fold difference in the IC_{50} values obtained for the two inhibitors.

Keywords: anti-allergy/crystal structure/hematopoietic prostaglandin (PG) D synthase (H-PGDS)/inhibitor/structure–function relationship.

Abbreviations: APAS, 1-amino-4-(4-aminosulphonyl)-phenyl-anthraquinone-2-sulphonic acid; BSPT, 2-(2′-benzothiazolyl)-5-styryl-3-(4′-phthalhydrazidyl) tetrazolium chloride; Cibacrone Blue, 1-Amino-4-{4-[4-chloro-6-(2-sulpho-phenylamino)-[1,3,5]triazin-2-ylmethyl]-3-sulpho-phenylamino}-9,10-dioxo-9,10-dihydro-anthracene-2-sulphonic acid; EDTA, ethylenediaminetetraacetic acid; EGTA, ethylene glycol tetraacetic acid; GSH, glutathione; H-PGDS, hematopoietic prostaglandin D synthase; PG, prostaglandin; PGD_2, prostaglandin D_2; PGH_2, prostaglandin H_2.

Prostaglandin D_2 (PGD_2), a metabolite of arachidonic acid (*1*, *2*), is a lipid mediator involved in sleep patterns (*3*, *4*) and inflammatory responses (*5*). PGD_2 activates two different types of receptors: DP1 (*6*) and DP2 [also known as CRTH2 (*7*)]. PGD_2 regulates sleep (*4*, *8*) and pain (*9*) via DP1 receptors in the central nervous system. This prostanoid also causes contraction of smooth airway muscle via DP1 receptors (*10*) and mediates chemotaxis of eosinophils and basophils into the lung via DP2 receptors (*11*) in the peripheral blood. Hence, PGD_2 coordinates and regulates allergic reactions, especially airway inflammation, via these two receptors (*11*).

Hematopoietic PGD synthase (H-PGDS) is isomerized from PGH_2 to produce PGD_2, which is an allergic mediator (*12*–*14*). Overproduction of PGD_2 has been shown to exacerbate asthmatic reactions, in an ovalbumin-challenged asthma model of human lipocalin-type PGDS- (*15*–*18*) and in H-PGDS-transgenic mice (*19*). However, asthmatic reactions were shown to be weakened in a prostanoid-specific G-protein coupled receptor (DP receptor) gene-knockout mouse model (*10*). Thus, human H-PGDS appears to be a promising target for the design of anti-allergic and anti-inflammatory drugs.

The GSH-dependent H-PGDS was first isolated from rat spleen (*12*). The 198 amino acid residue protein is a Sigma class member of the glutathione S-transferase (GST) superfamily with a molecular mass of 23 kDa (*20*). The 2.3 Å resolution X-ray structure of rat H-PGDS revealed that the protein has a high level of structural similarity to σ-type GST from squid (*21*, *22*). H-PGDS has the three pockets named Pocket 1 (consists of Met99, Phe102 and Trp104), Pocket 2 (consists of Arg14, Asp96, Tyr152 and Ile155) and Pocket 3 (consists of Lys112 and Lys198) at the active site; however, the enzymes of other GST family members do not have pocket 3 (*21*, *23*). Mutation of residues around the active site pocket

revealed that Trp104, a residue located at the ceiling of the active site pocket, was critical for structural integrity of the catalytic centre of GST and PGDS activity (*24*). Further analysis showed that Lys112 and Lys198, which were located at Pocket 3, were involved in recognition of the PGH_2 α-chain (*24*). We determined that the Ca^{2+}- and Mg^{2+}-bound human H-PGDS native structures had resolutions of 1.8 and 1.7 Å, respectively (*25*). We also explored the mechanism by which human H-PGDS was activated by Ca^{2+} and Mg^{2+} divalent cations by measuring their EC_{50} values; they were 400 and 50 μM, respectively (*25*). We next obtained the first H-PGDS inhibitor complex using 2-(2′-benzothiazolyl)-5-styryl-3-(4′-phthalhydrazidyl) tetrazolium chloride (BSPT) (*25*, *26*) The 1.9 Å resolution structure of the BSPT complex demonstrated how the inhibitor activity was influenced by the presence or absence of divalent metal ions (*26*). In further experiments, we determined the H-PGDS complex structure with the specific inhibitor HQL-79 (*27*). This inhibitor has shown a therapeutic effect when used in animal models of allergic disease (*28*, *29*), neuroinflammation (*30*) and muscular necrosis (*31*).

Like other GSTs, H-PGDS can also be inhibited by non-substrate ligands, such as haematin, organotin compounds and Cibacron Blue (1-Amino-4-{4-[4-chloro-6-(2-sulpho-phenylamino)-[1,3,5]triazin-2-ylmethyl]-3-sulpho-phenylamino}-9,10-dioxo-9,10-dihydro-anthracene-2-sulphonic acid); the IC_{50} value of the latter being 30 nM for chicken H-PGDS (*32*). Recent biochemical and structural characterization of novel inhibitors including Cibacron Blue and Nocodazole have determined the IC_{50} value for Cibacron Blue at of 200 nM [as calculated from the rates of conjugation activity in the presence of 1-chloro-2,4-dinitro benzene (CDNB)] (*33*). We report here on the measurement of the inhibitor activities of Cibacron Blue and 1-amino-4-(4-aminosulphonyl) phenyl-anthraquinone-2-sulphonic acid (APAS), two inhibitors of human H-PGDS, using PGH_2 as substrate. Both inhibitors are derived from the same compound, anthraquinone, but APAS lacks two aromatic rings. We found that the inhibitor activity of Cibacron Blue was ~50-fold higher than APAS, with an IC_{50} value of 40 nM. We discuss how correlations between X-ray structure and inhibitor activity profiles can provide valuable insight into design strategies for development of anti-allergy or anti-inflammatory therapeutic agents.

Experimental Procedures

H-PGDS inhibitor assays

All reagents containing Cibacron Blue and APAS were of analytical grade (Fig. 1A and B). Isolation and purification of human H-PGDS was carried out using previously reported methods (*23*, *34*). H-PGDS activity was measured using 40 μM [1-^{14}C] PGH_2 as substrate in a solution containing 0.1 M Tris–HCl (pH 8.0), 2 mM GSH and 0.1 mg/ml IgG, in the presence of ethylenediaminetetraacetic acid (EDTA)/ethylene glycol tetra-acetic acid (EGTA) or Ca^{2+}, with various concentrations of Cibacron Blue and APAS inhibitors. The products were separated by thin layer chromatography. The conversion rate for ^{14}C-labelled substrate to ^{14}C-labelled products was calculated using an imaging plate system (GE Healthcare). Kinetic constants were determined using Lineweaver–Burk plots prepared with SigmaPlot software (version 10.0 for Windows; Systat Software, Inc.).

Crystallography

Crystals of human H-PGDS, complexed with Cibacron Blue or APAS were obtained by co-crystallization using inhibitor concentrations of up to 100 μM in the presence of 5 mM Ca^{2+} at 20°C. No crystal complex of sufficiently high quality was obtained in the presence of Mg^{2+}. The X-ray diffraction data sets for the crystal complexes with either Cibacron Blue or APAS were collected at SPring-8 beam-lines 38B1 and 44XU, respectively (Table I). Cibacron Blue and APAS diffraction data were integrated and scaled with *HKL2000* (*35*) and *d*TREK* (*36*), respectively. The molecular replacement method for structure analyses was conducted using the Ca^{2+}-bound native structure as the starting model with the *AMoRe* program (*37*). Model re-building was performed using *COOT* (*38*), and the complex structure was refined by the *CNS* (*39*) and refmac5 (*40*): 5% of the reflections were set aside for R_{free} calculations (*41*). Ordered water molecules were included by selecting the peaks based on $F_{obs} - F_{calc}$ difference Fourier maps contoured at 2.5σ and $2F_{obs} - F_{calc}$ maps contoured at 1.2σ. The quality of the models was assessed from Ramachandran plots, and the model geometry analyses conducted using *PROCHECK* (*42*). The results of the data collection and refinement of the Cibacron Blue and APAS structure complexes are summarized in Table I.

Results

Effect of Ca^{2+} on the inhibitor activities of Cibacron Blue and APAS

Table II shows the effect of Ca^{2+} on the IC_{50} values of Cibacron Blue and APAS. While the IC_{50} value of Cibacron Blue was 40 nM in the presence of EDTA/EGTA, the value 150 nM was recorded in the presence of Ca^{2+} (Fig. 2A). In contrast, the IC_{50} values for APAS were 2.1 and 3.2 μM in the presence of EDTA/EGTA and Ca^{2+}, respectively (Fig. 2C). The IC_{50} values of both Cibacron Blue and APAS increased in the presence of Ca^{2+}. Comparison of the structure formulas of Cibacron Blue and APAS indicates that the additional two aromatic rings present in

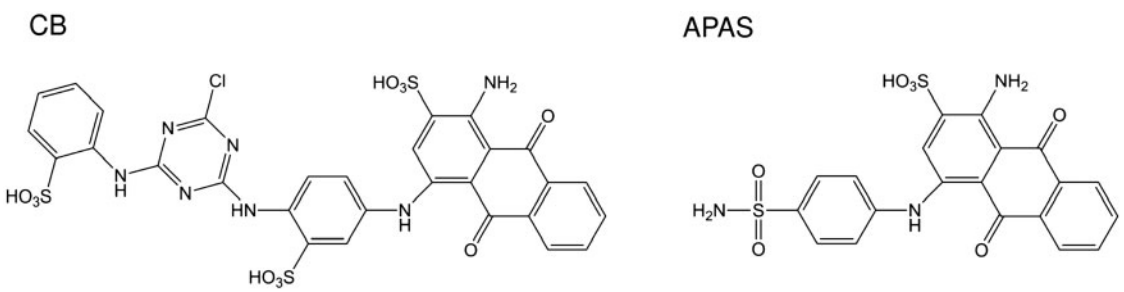

Fig. 1 Structure formulas of Cibacron Blue (CB) and APAS.

Table I. Data collection and refinement statistics for the complex of Cibacron Blue and APAS.

	Cibacron Blue	APAS
Inhibitor		
Metal ion	Ca^{2+}	Ca^{2+}
Space group	$P2_1$	$P1$
X-ray source	SPring-8 BL38B1	SPring-8 BL44XU
Max resolution (Å)	2.0	2.0
No. of flames	250	400
Oscillation angles (deg.)	1.1–1.5	0.5
Measured/unique reflections	212,706/57,344	116,777/53,869
Redundancy	2.1 (2.1)	2.1 (2.0)
Cell dimensions (Å, deg.)	$a=49.0$, $b=47.4$, $c=184.9$ $\beta=97.4$	$a=47.3$, $b=49.0$, $c=91$ $\alpha=95.8$, $\beta=91.0$, $\gamma=90.1$
Completeness (%)	98.1 (99.2)	97.0 (91.6)
Mean $<I/\Sigma/I>$	19.5 (4.8)	9.1 (2.2)
R_{merge}[a] (%)	6.8 (28.3)	5.3 (18.3)
Refinement statistics		
Resolution range (Å)	45.9–2.00	33.9–2.00
No. of GSH/inhibitor	4/2	2/2
No. of water/glycerol	743/0	699/1
R_{cryst}[b] (%)/R_{free}[c] (%)	17.4/23.3	17.6/24.9
Average B-factor (Å^2)		
GSH/inhibitor	32.8/81.0	40.6/52.4
R.m.s.d. deviation from ideal structures		
Bonds length (Å)	0.024	0.024
Angles (deg.)	1.9	1.8

Values in parentheses refer to the outermost shells (Cibacron Blue, 2.07–2.00 Å; APAS, 2.07–2.00 Å).
[a] $R_{merge}=\Sigma_j\Sigma_h\ |I_{h,j}-<I_h>|/\Sigma_j\Sigma_h\ <I_h>$.
[b] $R_{cryst}=\Sigma\ ||F_o|-|F_c||/\Sigma|F_o|$ calculated from 95% of the data, which were used during the course of the refinement.
[c] $R_{free}=\Sigma\ ||F_o|-|F_c||/\Sigma|F_o|$, calculated from 5% of the data, which were used during the course of the refinement.

Table II. IC_{50} values of the inhibitor compounds.

	Cibacron Blue	APAS
2 mM EDTA	40.4 ± 2.6 (nM)	2.1 ± 0.31 (μM)
2 mM Ca^{2+}	150 ± 11 (nM)	3.2 ± 0.27 (μM)

the Cibacron Blue molecule may have been responsible for the dramatic changes observed in the inhibition activity of this compound.

Kinetic analysis of H-PGDS inhibition against GSH by Cibacron Blue or APAS

Kinetic analysis using the human H-PGDS in the presence of 2 mM Ca^{2+} revealed that Cibacron Blue inhibited the H-PGDS activity in a non-competitive manner against GSH, giving a K_i of 87.5 nM (Fig. 2B). On the other hand, APAS inhibited the H-PGDS in a competitive manner against GSH with a K_i of 2.5 μM (Fig. 2D). These results indicate that Cibacron Blue did not bind to the GSH-binding site, but APAS bound to the GSH-binding site.

Structure of the Cibacron Blue–human H-PGDS complex

We obtained the crystal of human H-PGDS complexed with Cibacron Blue in a monoclinic space group of $P2_1$ like the Ca^{2+}-bound native crystal at pH 8.4 (*25*), and determined the complex structure at a resolution of 2.0 Å. The structure showed that two dimer molecules were contained in an asymmetric unit. From the viewpoint of the crystal packing, Mol-A (Mol-A′) and Mol-B (Mol-B′) categorize the outside molecules of each of the dimers, whereas Mol-C (Mol-C′) and Mol-D (Mol-D′) are the inside molecules of it (*26*). While one GSH molecule was found in each of the active sites derived from four independent molecules, the Cibacron Blue molecule was only found in the outside molecules, Mol-A′ and Mol-B′; some weak residual electron density from the inhibitor was apparent in the inside molecules, Mol-C′ and Mol-D′ (*26*). The superimposition between the outside molecules (Mol-A′ and Mol-B′), and between the inside molecules (Mol-C′ and Mol-D′) showed small averaged root mean square (r.m.s.d.'s) deviations of 0.27 and 0.35 Å, respectively, for the whole C_α carbon atoms; the r.m.s.d.'s for the other combinations increased to 0.48 Å. The Cibacron Blue-bound Mol-A/Mol-D and Mol-B/Mol-C complexes were heterogeneous (Fig. 3A).

Inspection of the electron density map showed that the benzenesulphonic group adjacent to the anthraquinone hydrogen bonded with both the amido group of GSH and Gln36 through a water molecule (Fig. 3B and C). Cibacron Blue was also stabilized by hydrogen bonds between the terminal sulphate group and Lys112 and Lys198, but the electron density was poor (Fig. 3C and D). Moreover, the Cibacron Blue molecule was stabilized by a π–π interaction between the anthraquinone ring and Trp104. In contrast, the following four van der Waals contacts were observed; (i) between Nε (Arg14) and the 1-amino group, (ii) between Nε (Arg14) and the quinone group, (iii) between the NH1 (Arg14) and the quinone group and

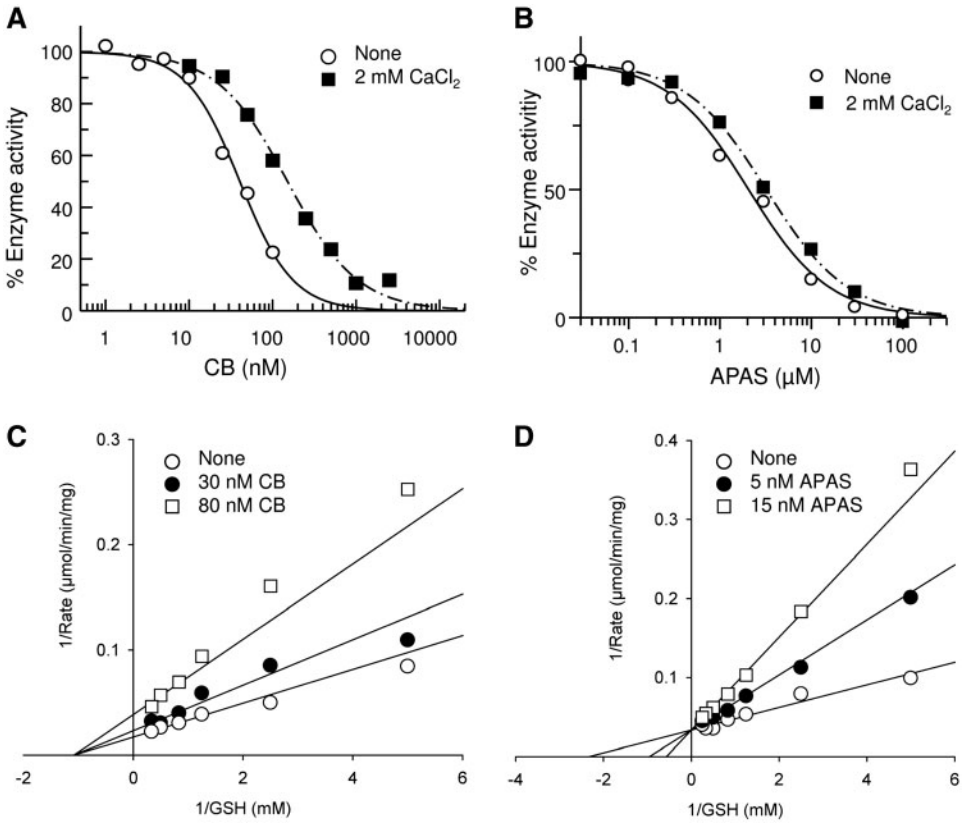

Fig. 2 Kinetic analysis of H-PGDS inhibition by Cibacron Blue (CB) and APAS. Enzyme activities were determined in the presence of various concentrations of CB (A) and APAS (B). H-PGDS activity was measured in the presence or absence of 2 mM $CaCl_2$. Lineweaver–Burk plots of H-PGDS activity in the presence of various concentrations of CB (C) or APAS (D).

(iv) between the carbonyl group of GSH and the 2-sulphonic group in the anthraquinone ring. However, these four hydrogen bonds and the π–π interaction contribute to the lowest IC_{50} value observed in the presence of EDTA/EGTA (i.e. 40 nM; Fig. 2C).

Structure of the APAS–human H-PGDS complex

We obtained an APAS-bound complex that had a different crystal form with *P*1 in the presence of Ca^{2+}, and determined the complex structure at a resolution of 2.0 Å. From this crystal complex, we detected two dimer molecules, i.e. Mol-A and Mol-D, and Mol-C and Mol-B, in an asymmetrical unit (*26*). The averaged r.m.s.d.'s for all of the C_α carbon atoms between the outside molecules, Mol-A and Mol-B, and the inside molecules, Mol-C and Mol-D, were calculated at 0.28 and 0.10 Å, respectively. However, values of more than 0.45 Å for other combinations amongst the four independent molecules (Mol-A/Mol-B and Mol-C/Mol-D) were obtained. We found that the inhibitor molecules predominantly bound to the inner molecules of Mol-C and Mol-D, even when some weak residual electron density of the inhibitor was found in the outside molecules of Mol-A and Mol-B. Heterogeneity of the structures between the protomers in the dimer was also observed (Fig. 4A).

Superimposition between the inner and the outer molecules of the APAS-bound complex showed that a movement had occurred around the α5-helix upon APAS binding (Fig. 5). The C_α (Gln109) atomic distance between the inner and the outer molecules was 1.6 Å, whereas C_α (Val199) was 0.13 Å. The movement of Gln109 is remarkable because of the small averaged r.m.s.d. of 0.45 Å for the superimposition. Interestingly, the Gln109 (C_α)–Val199 (C_α) atomic distance changed from 17.8 Å to 16.1 Å upon binding of APAS. The closure of the active site was due to the movement of the α5-helix containing Gln109. The Gln109 movement was also observed in the Cibacron Blue bound complex (2.1 Å); however, the change of the crystal form from $P2_1$ to *P*1 was only observed upon binding of APAS in the presence of Ca^{2+}. This change may be because APAS, which is smaller than Cibacron Blue, may have only been able to bind to the inside molecules.

The electron density profile of the APAS molecule is shown in Fig. 4B. It is apparent that the inhibitor molecule is stabilized by the hydrogen bond between the 2-sulphonic group and Lys112 through a water molecule, and by the stacking interaction with Trp104 (Fig. 4C and D). Two van der Waals contacts between Nε (Arg14) and the quinone group, and between NH1 (Arg14) and the quinone group, were observed. The benzenesulphonic group was affected by steric hindrance with the bound GSH molecule, reducing the electron density for GSH within the inside molecules of Mol-C and Mol-D. The complex structure also

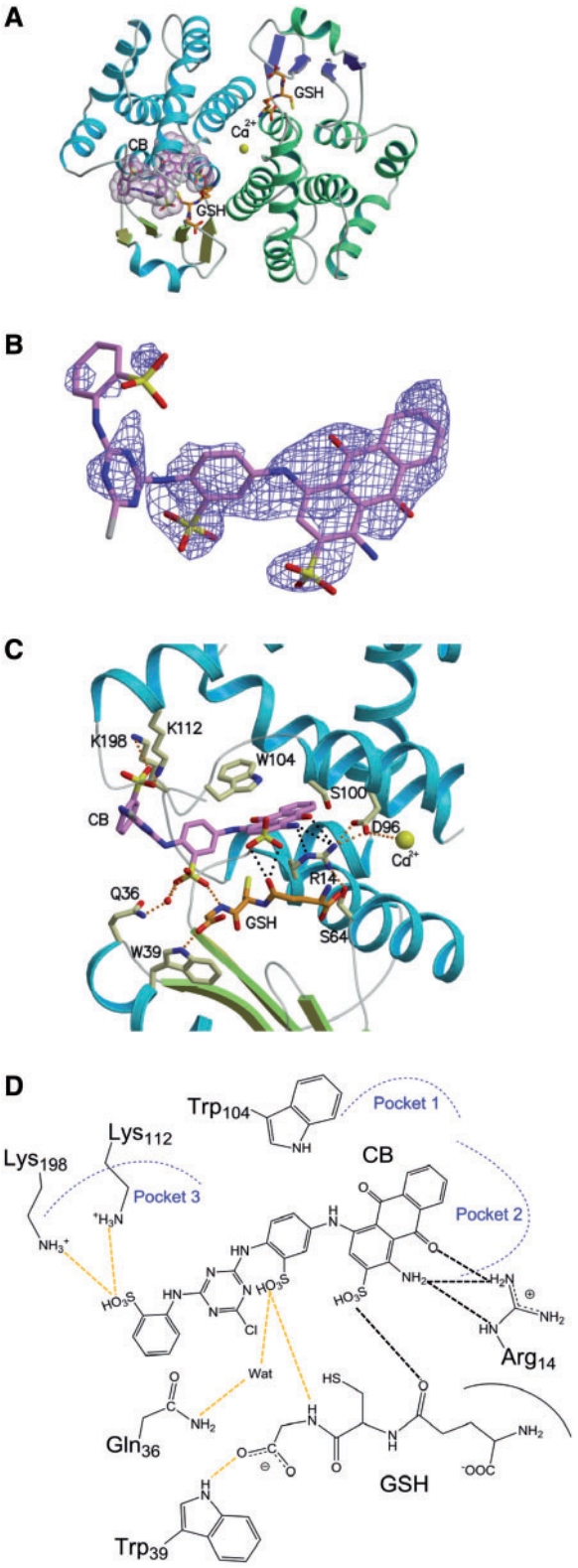

Fig. 3 The structure of the Cibacron Blue-bound complex. (A) The Cibacron Blue inhibitor molecule binds to the outside molecule, Mol-A (cyan), not to the inside molecule, Mol-D (green), while the GSH cofactor molecule binds to both molecules in the dimer. (B) The $(2F_o - F_c)$ omit map around the Cibacron Blue inhibitor is represented at the 1.2σ-level. (C) A close-up view of the active site structure showing that the inhibitor was stabilized by a π–π stacking interaction between the anthraquinone ring and Trp104, and also by four hydrogen bonds (dotted orange line). However, van der Waals contacts were also found (dotted black line). (D) The hydrogen bond network around the Cibacron Blue molecule has been drawn schematically.

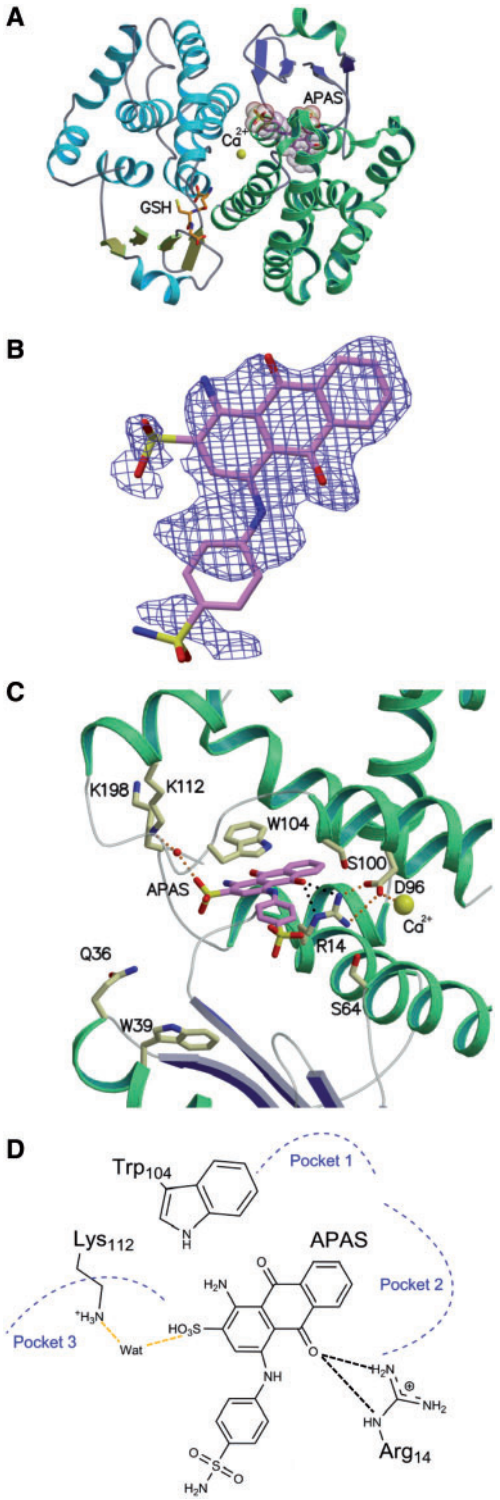

Fig. 4 The structure of the APAS-bound complex. (A) The APAS inhibitor molecule and GSH cofactor molecule bind to Mol-D (green) and Mol-A (cyan), respectively. (B) The $(2F_o - F_c)$ omit map around the APAS inhibitor is contoured at the 1.2σ-level. (C) A close-up view of the active site structure. The APAS anthraquinone ring is in an oppositely bound configuration to the H-PGDS active site compared to the same ring in Cibacron Blue. The APAS benzenesulphonic group has steric hindrance with GSH, making the GSH molecule appear to disappear from the H-PGDS active site. The inside monomer, Mol-D, only binds to APAS, not to GSH; conversely, the outside monomer, Mol-A, only binds to GSH, not to APAS. The inhibitor is stabilized by a π–π stacking interaction between the anthraquinone ring and Trp104, and by a salt-bridge between the 2-sulphonic group and Lys112 via a water molecule (dotted orange line). (D) The interactions between the APAS molecule and the H-PGDS active site are schematically drawn.

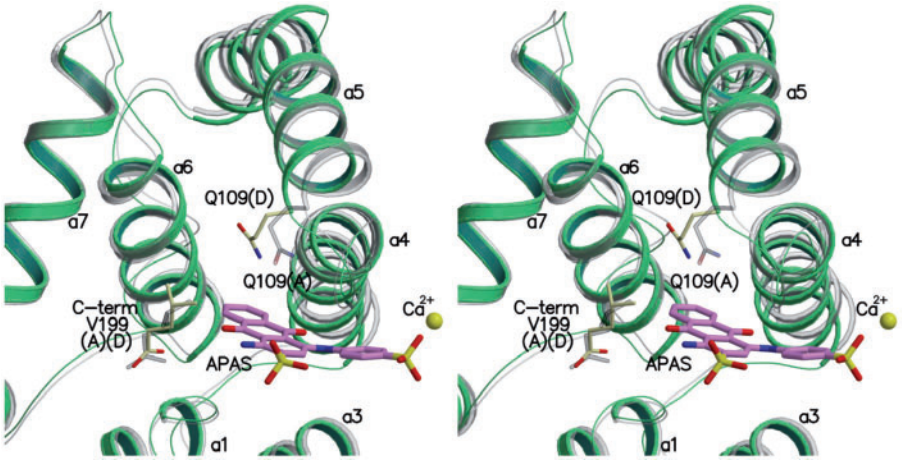

Fig. 5 Stereo figures of the structural comparison between the monomers in the APAS-bound complex. Mol-D in the APAS bound complex (green) was superimposed on Mol-A (grey), showing that the Cα atom of Gln109 moved by 1.6 Å because of the induced-fit of the α5-helix upon binding of APAS. The figure shows a view from the left-hand side of Fig. 4C.

revealed that APAS was competitive with GSH. Some APAS may also bind to the outside molecules. As a result, the average B-factor for GSH in the active site of the outside molecules (Mol-A and Mol-B) was 40.6 $Å^2$, a value that is relatively larger than the averaged B-factor for whole structure of the outside molecules.

Discussion

Our experiments show that the inhibitor activity of Cibacron Blue, at 40 nM, represents a 50-fold increase over the value obtained for APAS in the presence of EDTA/EGTA (Table II). We also observed that the Cibacron Blue terminal sulphonate group was hydrogen bonded with the conserved residues of Lys112 and Lys198. In previous work, we showed that the catalytic pocket of H-PGDS comprised three distinct pockets. One of the pockets at the active site, Pocket 3 (containing Lys112 and Lys198), was involved in the recognition of the PGH_2 α-chain (*23*, *24*). It is possible, therefore, that the Cibacron Blue terminal sulphate group blocks the Lys112 and Lys198 functional residues. However, the APAS molecule could not directly interact with the Lys112 and Lys198 in H-PGDS, because it lacks the two aromatic rings present in Cibacron Blue. Instead, the 2-sulphonic group interacted with Lys112 through a water molecule. Therefore, the structure-based design to acquire direct hydrogen bonding with Lys112 and Lys198 in Pocket 3 could result in a potential 50-fold inhibition of activity improvement.

The IC_{50} value for APAS was measured at 2.1 μM in the presence of EDTA/EGTA; however, the IC_{50} value increased 1.5-fold in the presence of Ca^{2+} (Table II). In our previous report, the K_m value of the substrate, PGH_2, decreased 1.4-fold in the presence of Ca^{2+} (*25*). Because APAS competes for binding to PGH_2, the 1.5-fold increase in the IC_{50} value corresponds well with the increase in affinity for PGH_2 in the presence of Ca^{2+}.

On the other hand, the data for Cibacron Blue revealed that the IC_{50} value for this compound also increased in the presence of Ca^{2+}. However, the obtained value was higher than that of APAS in the presence of Ca^{2+} (3.7-fold; Table II). When the Cibacron Blue anthraquinone group penetrated into the active site, the break of hydrogen bond network containing Arg14 was observed (Fig. 6). The distances of NH1 (Arg14)-Oγ (Ser100) and NH2 (Arg14)-Oγ (Ser64) were 4.1 and 2.7 Å, respectively, in the presence of Cibacron Blue, and those values were 3.8 and 3.4 Å in the presence of APAS, respectively, while those averaged distances were recorded to be 2.8 and 4.0 Å, respectively, in the Ca^{2+}-bound native structure. It is possible, therefore, that the cause of the stronger metal ion effect on the inhibition activity is related to the break of the hydrogen bond network found in Cibacron Blue complex.

A fragment-based drug design approach was recently examined using a number of new inhibitors that bind within the active site cavity of H-PGDS without inducing conformational changes (*43*). Nevertheless, our study highlights a novel strategy that could be exploited for inhibitor design in which a human H-PGDS inhibitor could interact with Lys112 and Lys198 in Pocket 3 without any steric hindrance against the Arg14 residue and the bound GSH molecule. Such a strategy may prove useful for further development of anti-allergic or anti-inflammatory drugs.

Acknowledgements

The authors are grateful to Dr. Daisuke Irikura and Mr. Shigehiro Kinugasa for their kind support with the purification of sample and the crystallization of complex. The authors express their appreciation to all the staffs for their kind support with the data collection at the SPring-8 beam-line 38B1 and 44XU, and to Emeritus Prof. Osamu Hayaishi, Osaka Bioscience Institute, for his generous support.

Funding

This study was supported by the Grants-in-Aid for Scientific Research (No. 22550152) from the Ministry of Education, Culture, Sports, Science and Technology of Japan and PRESTO project, Japan Science and Technology Agency and Technology

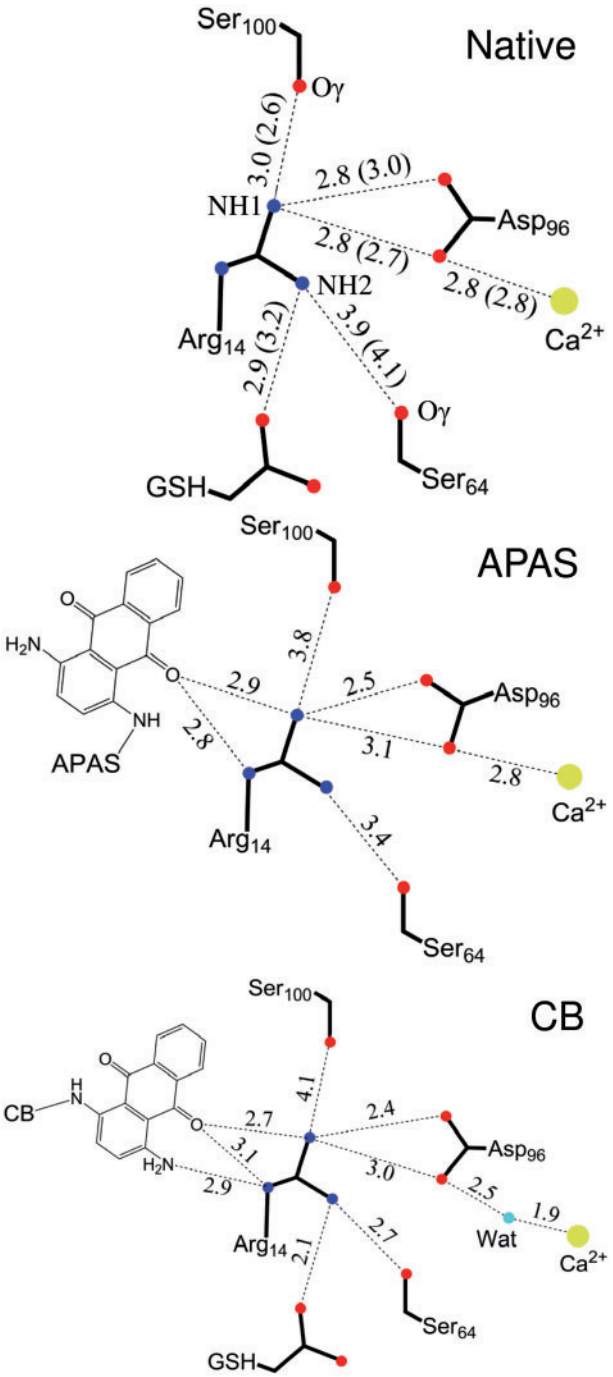

Fig. 6 Schematic drawing of the Native, APAS-bound and Cibacron Blue-bound form of H-PGDS around Arg14. Blue balls depict nitrogen atoms and red balls oxygen atoms. The unit value is Å. Values shown in parenthesis represent the mean values for the inner (Mol-C and Mol-D) and those without parenthesis for outer molecules (Mol-A and Mol-B) in the native protein diagram. The distance between Ser100 and Arg14 for the native form, APAS-bound form and CB-bound form are in ascending order according to length.

Corporation, partly by the National Project on Protein Structural and Functional Analyses, Japan (to T. I.), JAXA (Japan Aerospace Exploration Agency), TAIHO Pharmaceutical Co., Ltd., Takeda Pharmaceutical Co., Ltd. and Ono Pharmaceutical Co., Ltd. (to Y.U. and K.A.).

Conflict of interest
None declared.

References

1. Giles, H. and Leff, P. (1988) The biology and pharmacology of PGD2. *Prostaglandins* **35**, 277–300
2. Ito, S., Narumiya, S., and Hayaishi, O. (1989) Prostaglandin D2: a biochemical perspective. *Prostaglandins Leukot. Essent. Fatty Acids* **37**, 219–234
3. Ueno, R., Ishikawa, Y., Nakayama, T., and Hayaishi, O. II (1982) Prostaglandin D2 induces sleep when microinjected into the preoptic area of conscious rats. *Biochem. Biophys. Res. Commun.* **109**, 576–582
4. Qu, W.M., Huang, Z.L., Xu, X.H., Aritake, K., Eguchi, N., Nambu, F., Narumiya, S., Urade, Y., and Hayaishi, O. (2006) Lipocalin-type prostaglandin D synthase produces prostaglandin D2 involved in regulation of physiological sleep. *Proc. Natl Acad. Sci. USA* **103**, 17949–17954
5. Lewis, R.A., Soter, N.A., Diamond, P.T., Austen, K.F., Oates, J.A., and Roberts, L.J. II. (1982) Prostaglandin D2 generation after activation of rat and human mast cells with anti-IgE. *J. Immunol.* **129**, 1627–1631
6. Hirata, M., Kakizuka, A., Aizawa, M., Ushikubi, F., and Narumiya, S. (1994) Molecular characterization of a mouse prostaglandin D receptor and functional expression of the cloned gene. *Proc. Natl Acad. Sci. USA* **91**, 11192–11196
7. Nagata, K., Hirai, H., Tanaka, K., Ogawa, K., Aso, T., Sugamura, K., Nakamura, M., and Takano, S. (1999) CRTH2, an orphan receptor of T-helper-2-cells, is expressed on basophils and eosinophils and responds to mast cell-derived factor(s). *FEBS Lett.* **459**, 195–199
8. Mizoguchi, A., Eguchi, N., Kimura, K., Kiyohara, Y., Qu, W.M., Huang, Z.L., Mochizuki, T., Lazarus, M., Kobayashi, T., Kaneko, T., Narumiya, S., Urade, Y., and Hayaishi, O. (2001) Dominant localization of prostaglandin D receptors on arachnoid trabecular cells in mouse basal forebrain and their involvement in the regulation of non-rapid eye movement sleep. *Proc. Natl Acad. Sci. USA* **98**, 11674–11679
9. Eguchi, N., Minami, T., Shirafuji, N., Kanaoka, Y., Tanaka, T., Nagata, A., Yoshida, N., Urade, Y., Ito, S., and Hayaishi, O. (1999) Lack of tactile pain (allodynia) in lipocalin-type prostaglandin D synthase-deficient mice. *Proc. Natl Acad. Sci. USA* **96**, 726–730
10. Matsuoka, T., Hirata, M., Tanaka, H., Takahashi, Y., Murata, T., Kabashima, K., Sugimoto, Y., Kobayashi, T., Ushikubi, F., Aze, Y., Eguchi, N., Urade, Y., Yoshida, N., Kimura, K., Mizoguchi, A., Honda, Y., Nagai, H., and Narumiya, S. (2000) Prostaglandin D2 as a mediator of allergic asthma. *Science* **287**, 2013–2017
11. Hirai, H., Tanaka, K., Yoshie, O., Ogawa, K., Kenmotsu, K., Takamori, Y., Ichimasa, M., Sugamura, K., Nakamura, M., Takano, S., and Nagata, K. (2001) Prostaglandin D2 selectively induces chemotaxis in T helper type 2 cells, eosinophils, and basophils via seven-transmembrane receptor CRTH2. *J. Exp. Med.* **193**, 255–261
12. Christ-Hazelhof, E. and Nugteren, D.H. (1979) Purification and characterisation of prostaglandin endoperoxide D-isomerase, a cytoplasmic, glutathione-requiring enzyme. *Biochim. Biophys. Acta* **572**, 43–51
13. Urade, Y., Fujimoto, N., Ujihara, M., and Hayaishi, O. (1987) Biochemical and immunological characterization of rat spleen prostaglandin D synthetase. *J. Biol. Chem.* **262**, 3820–3825
14. Urade, Y., Mohri, I., Aritake, K., Inoue, T., and Miyano, M. (2006) Biochemical and structural

characteristics of hematopoietic prostaglandin D synthase: From evolutionary analysis to drug designing in *Functional and Structural Biology on the Lipo-network* (Morikawa, K. and Tate, S., eds.), pp. 135–164, Transworld Research Network, Kerala, India.

15. Urade, Y., Fujimoto, N., and Hayaishi, O. (1985) Purification and characterization of rat brain prostaglandin D synthetase. *J. Biol. Chem.* **260**, 12410–12415
16. Urade, Y., Eguchi, N., and Hayaishi, O. (2006) Lipocalin-type prostaglandin D synthase as an enzymic lipocalin. *Lipocalins* **9**, 99–109
17. Nagata, A., Suzuki, Y., Igarashi, M., Eguchi, N., Toh, H., Urade, Y., and Hayaishi, O. (1991) Human brain prostaglandin D synthase has been evolutionarily differentiated from lipophilic-ligand carrier proteins. *Proc. Natl Acad. Sci. USA* **88**, 4020–4024
18. Urade, Y. and Hayaishi, O. (2000) Biochemical, structural, genetic, physiological, and pathophysiological features of lipocalin-type prostaglandin D synthase. *Biochim. Biophys. Acta* **1482**, 259–271
19. Fujitani, Y., Kanaoka, Y., Aritake, K., Uodome, N., Okazaki-Hatake, K., and Urade, Y. (2002) Pronounced eosinophilic lung inflammation and Th2 cytokine release in human lipocalin-type prostaglandin D synthase transgenic mice. *J. Immunol.* **168**, 443–449
20. Hayes, J.D. and Pulford, D.J. (1995) The glutathione S-transferase supergene family: regulation of GST and the contribution of the isoenzymes to cancer chemoprotection and drug resistance. *Crit. Rev. Biochem. Mol. Biol.* **30**, 445–600
21. Kanaoka, Y. and Urade, Y. (2003) Hematopoietic prostaglandin D *synthase*. *Prostaglandins Leukot. Essent. Fatty Acids* **69**, 163–167
22. Ji, X., von Rosenvinge, E.C., Johnson, W.W., Tomarev, S.I., Piatigorsky, J., Armstrong, R.N., and Gilliland, G.L. (1995) Three-dimensional structure, catalytic properties, and evolution of a sigma class glutathione transferase from squid, a progenitor of the lens S-crystallins of cephalopods. *Biochemistry* **34**, 5317–5328
23. Kanaoka, Y., Ago, H., Inagaki, E., Nanayama, T., Miyano, M., Kikuno, R., Fujii, Y., Eguchi, N., Toh, H., Urade, Y., and Hayaishi, O. (1997) Cloning and crystal structure of hematopoietic prostaglandin D synthase. *Cell* **90**, 1085–1095
24. Pinzar, E., Miyano, M., Kanaoka, Y., Urade, Y., and Hayaishi, O. (2000) Structural basis of hematopoietic prostaglandin D synthase activity elucidated by site-directed mutagenesis. *J. Biol. Chem.* **275**, 31239–31244
25. Inoue, T., Irikura, D., Okazaki, N., Kinugasa, S., Matsumura, H., Uodome, N., Yamamoto, M., Kumasaka, T., Miyano, M., Kai, Y., and Urade, Y. (2003) Mechanism of metal activation of human hematopoietic prostaglandin D synthase. *Nat. Struct. Biol.* **10**, 291–296
26. Inoue, T., Okano, Y., Kado, Y., Aritake, K., Irikura, D., Uodome, N., Okazaki, N., Kinugasa, S., Shishitani, H., Matsumura, H., Kai, Y., and Urade, Y. (2004) First determination of the inhibitor complex structure of human hematopoietic prostaglandin D synthase. *J. Biochem.* **135**, 279–283
27. Aritake, K., Kado, Y., Inoue, T., Miyano, M., and Urade, Y. (2006) Structural and functional characterization of HQL-79, an orally selective inhibitor of human hematopoietic prostaglandin D synthase. *J. Biol. Chem.* **281**, 15277–15286
28. Matsushita, N., Aritake, K., Takada, A., Hizue, M., Hayashi, K., Mitsui, K., Hayashi, M., Hirotsu, I., Kimura, Y., Tani, T., and Nakajima, H. (1998) Pharmacological studies on the novel antiallergic drug HQL-79: II. Elucidation of mechanisms for antiallergic and antiasthmatic effects. *Jpn. J. Pharmacol.* **78**, 11–22
29. Matsushita, N., Hizue, M., Aritake, K., Hayashi, K., Takada, A., Mitsui, K., Hayashi, M., Hirotsu, I., Kimura, Y., Tani, T., and Nakajima, H. (1998) Pharmacological studies on the novel antiallergic drug HQL-79: I. Antiallergic and antiasthmatic effects in various experimental models. *Jpn. J. Pharmacol.* **78**, 1–10
30. Mohri, I., Taniike, M., Taniguchi, H., Kanekiyo, T., Aritake, K., Inui, T., Fukumoto, N., Eguchi, N., Kushi, A., Sasai, H., Kanaoka, Y., Ozono, K., Narumiya, S., Suzuki, K., and Urade, Y. (2006) Prostaglandin D2-mediated microglia/astrocyte interaction enhances astrogliosis and demyelination in twitcher. *J. Neurosci.* **26**, 4383–4393
31. Mohri, I., Aritake, K., Taniguchi, H., Sato, Y., Kamauchi, S., Nagata, N., Maruyama, T., Taniike, M., and Urade, Y. (2009) Inhibition of prostaglandin D synthase suppresses muscular necrosis. *Am. J. Pathol.* **174**, 1735–1744
32. Thomson, A.M., Meyer, D.J., and Hayes, J.D. (1998) Sequence, catalytic properties and expression of chicken glutathione-dependent prostaglandin D2 synthase, a novel class Sigma glutathione S-transferase. *Biochem. J.* **333**, 317–325
33. Weber, J.E., Oakley, A.J., Christ, A.N., Clark, A.G., Hayes, J.D., Hall, R., Hume, D.A., Board, P.G., Smythe, M.L., and Flanagan, J.U. Identification and characterisation of new inhibitors for the human hematopoietic prostaglandin D2 synthase. *Eur. J. Med. Chem.* **45**, 447–454
34. Kanaoka, Y., Fujimori, K., Kikuno, R., Sakaguchi, Y., Urade, Y., and Hayaishi, O. (2000) Structure and chromosomal localization of human and mouse genes for hematopoietic prostaglandin D synthase. Conservation of the ancestral genomic structure of sigma-class glutathione S-transferase. *Eur. J Biochem.* **267**, 3315–3322
35. Otwinowski, Z. and Minor, W. (1993) Data Collection and Processing in *Proceedings of the CCP4 Study Weekend* (Sawyer, L., Issacs, N. and Bailey, S., eds.), pp. 56–62, Daresbury Laboratories, Warrington, United Kingdom.
36. Pflugrath, J.W. (1999) The finer things in X-ray diffraction data collection. *Acta Crystallogr. D Biol. Crystallogr.* **55**, 1718–1725
37. Navaza, J. (2001) Implementation of molecular replacement in AMoRe. *Acta Crystallogr. D Biol. Crystallogr.* **57**, 1367–1372
38. Emsley, P. and Cowtan, K. (2004) Coot: model-building tools for molecular graphics. *Acta Crystallogr. D Biol. Crystallogr.* **60**, 2126–2132
39. Brunger, A.T., Adams, P.D., Clore, G.M., DeLano, W.L., Gros, P., Grosse-Kunstleve, R.W., Jiang, J.S., Kuszewski, J., Nilges, M., Pannu, N.S., Read, R.J., Rice, L.M., Simonson, T., and Warren, G.L. (1998) Crystallography & NMR system: A new software suite for macromolecular structure determination. *Acta Crystallogr. D Biol. Crystallogr.* **54 (Pt 5)**, 905–921
40. Murshudov, G.N., Skubak, P., Lebedev, A.A., Pannu, N.S., Steiner, R.A., Nicholls, R.A., Winn, M.D., Long, F., and Vagin, A.A. (2011) REFMAC5 for

the refinement of macromolecular crystal structures. *Acta Crystallogr. D Biol. Crystallogr.* **67**, 355–367

41. Brunger, A.T. (1992) Free R value: a novel statistical quantity for assessing the accuracy of crystal structures. *Nature* **355**, 472–475
42. Laskowsky, R.A. (1993) PROCHECK: a program to check the stereochemicai quality of protein structures. *J. Appl. Cryst.* **26**, 283–291
43. Hohwy, M., Spadola, L., Lundquist, B., Hawtin, P., Dahmen, J., Groth-Clausen, I., Nilsson, E., Persdotter, S., von Wachenfeldt, K., Folmer, R.H., and Edman, K. (2008) Novel prostaglandin D synthase inhibitors generated by fragment-based drug design. *J. Med. Chem.* **51**, 2178–2186